Acta Geologica Sinica (English Edition), 2025, 99(1): 243–257

Hydrothermal Control by Deep Hidden Faults on Geothermal Systems in Sedimentary Basins: A Case Study of the Cangdong Fault in the North China Basin

YIN Xiaoxiao[1, 2, 3], LIN Jianwang[1, 3, *], LI Hu[1, 2, 3], LI Huanqing[4], DONG Lufei[1, 2], YAN Jiaxian[1, 2, 3], ZHANG Sen[1, 2, 3] and LI Zheng[1, 2]

[1] *Tianjin Geothermal Exploration and Development Design Institute, Tianjin 300250, China*
[2] *Observation and Research Station of Tianjin Low-Medium Temperature Geothermal Resources, Ministry of Natural Resources, Tianjin 300250, China*
[3] *Technology Innovation Base for Geothermal Resource Development and Utilization, Tianjin 300250, China*
[4] *Tianjin Municipal Bureau of Planning and Natural Resources, Tianjin 300042, China*

Abstract: Large basins are currently the global focus for geothermal development, with their hydrothermal system being controlled by a variety of factors, such as basement relief and fracture development. Donglihu is located at the north of the Cangxian uplift in the North China Basin, the concentrated geothermal resource development zone in North China. This study systematically collects temperature logging data and long-term dynamic monitoring of water level and water quality as well as group well tracer test data carried out in this area in recent years, on the basis of which the hydrothermal controlling role of the deep hidden faults is systematically analyzed. The results show that the Cangdong fault communicates with different geothermal reservoirs in the shallow part and plays a specific role in the water-heat channel of the local area. As a result, the high-value area of the geothermal temperature gradient in the sedimentary layer of the Donglihu area is distributed around the Cangdong fault. The geothermal reservoir temperature of the Minghuazhen Formation within the influence of the fault is also significantly higher than the regional average, the hydraulic head of different geothermal reservoirs showing a consistent and synergistic trend. However, the water quality has been stable for many years without any apparent changes. This understanding has a particular significance for further deepening understanding of the geothermal genesis mechanism in sedimentary basins and guiding future geothermal exploration and development in the Donglihu area.

Key words: sedimentary basin geothermal system, hidden fault, hydrothermal channel, Cangdong fault

Citation: Yin et al., 2025. Hydrothermal Control by Deep Hidden Faults on Geothermal Systems in Sedimentary Basins: A Case Study of the Cangdong Fault in the North China Basin. Acta Geologica Sinica (English Edition), 99(1): 243–257. DOI: 10.1111/1755-6724.15263

1 Introduction

Geothermal, as a clean, low-carbon and widely distributed high-quality renewable energy, has a significant role in promoting global energy restructuring. In recent years, global geothermal development has made rapid progress, with the search for high-quality geothermal resources becoming the main task of geothermal development (Wang and Lin, 2020; Lin et al., 2021a, b; Long et al., 2023). Sedimentary basins are crucial geothermal resource areas. China has a large area of Mesozoic and Cenozoic sedimentary basins, in particular the North China Basin (NCB), Songliao basin, Jianghan basin, Subei basin, Guanzhong basin and other rift basins located in eastern China. These basins account for 89% of the currently exploitable hydrothermal geothermal resources in China and are the most exploitable and central heat-controlling geological units in China (Zhang et al., 2019).

Heat transfer in sedimentary basins occurs primarily by conduction and convection (Zhao et al., 2013; Qiu et al., 2019). The distribution of geothermal temperature is controlled and influenced by many factors, such as deep crustal structure, regional geological structure, magmatic and volcanic activities, as well as groundwater activities, which control or restrict the distribution of the temperature field and the formation of geothermal resources in the basin (Qiu et al., 2019; Wang G et al., 2023; Zhang et al., 2023; Wang L et al., 2024). The NCB is the most important sedimentary basin geothermal field in China, with some research work having been carried out on hydrothermal transport in this basin. Chen (1988) systematically analyzed the distribution of the geothermal field in the shallow part of the NCB, based on a large

* Corresponding author. E-mail: yinxiaoxiaogw@163.com

amount of petroleum borehole logging data. He proposed that the main factors affecting the distribution of temperature at depth include bedrock relief and tectonic morphology, groundwater activity and magmatic activity. Mao (2018) and Wang X W et al. (2022) further carried out temperature simulations, based on borehole logging data from the Niutuozhen uplift and Xianxian uplift in the basin, proposing that the non-uniformity of thermal conductivity is the determinant or main controlling factor in large-scale temperature distribution. Lin et al. (2022) compared deep-hole temperatures and crustal thermal structure in different parts of the Matouying uplift, suggesting that the hidden deep faults on the northwest side of the uplift communicate with the mantle heat source and constitute the primary heat source affecting shallow temperatures. Most of these studies are based on the use of borehole logging data to carry out comparative analysis of spatial temperature distribution, the majority of them focussing on the role of heat aggregation in the deep bedrock uplifts in the NCB, with little research has being done on the role of hidden faults developed in the deep basin. Although Zhao et al. (2007) carried out a study on hydrothermal control of the Cangdong fault at the base of the NCB, based on drilling practice, proposing that the Cangdong fault does not control the regional geothermal heat source, they lacked the supporting data of different geothermal reservoirs in the region. In recent years, with the implementation of large-scale geothermal water pumping-reinjection systems in the NCB, especially in the Tianjin area, as well as the continuous improvement of the dynamic routing monitoring system of geothermal reservoirs (Yin et al., 2024), the continuous accumulation of series data provides the possibility for in-depth analysis of the role of heat- and water-channels of the hidden faults in the basin.

Hidden faults are not exposed at the surface, but are hidden below it. The Cangxian uplift is located on the east side of the Jizhong depression in the NCB, with several geothermal anomalies and abundant geothermal resources, making it one of the most critical geothermal exploitation areas in North China (Chen and Wang, 1994; Wang T H et al., 2022; Shi et al., 2023). Several hidden faults have developed in the area (Hao et al., 2014), including the Cangdong fault on the east side of the Cangxian uplift and a significant hidden fault in the NCB. Based on steady-state logging and long-term water level and water quality monitoring data, as well as group well pumping-reinjection tracer tests conducted in the Donglihu area at the northern end of the Cangxian uplift in recent years, this study will systematically analyze the distribution and characteristics of the geothermal reservoirs in the area, analyzing the hydrothermal linkage and coupling effects between different reservoirs, as well as deeply exploring the water-heat channeling role of the deeply hidden Cangdong fault in the NCB, in order to provide a basis for guiding exploration and development of the geothermal resources in the area.

2 Geological Setting

The Donglihu area is located in the northeastern part of the NCB, its tectonic position lying on the Panzhuang uplift and the Beitang sag (Fig. 1). The Cangdong fault runs through the area in a north-east direction, as a compressive–torsional fracture in the axis of the backslope, with an NNE strike, an inclination of ESE and a dipping angle of 30°–48°, with a fault throw of 1,000–6,000 m. The western part of the fault is a relatively rising normal fault, which is the boundary between the Panzhuang uplift and the Beitang sag. To the west of the Cangdong fault is the Panzhuang uplift, where the bedrock is dominated by the Mesozoic, Paleozoic Cambrian and middle Neogene, the depth of the roof of the bedrock being 1430–1750 m. To the east of the Cangdong fault is the Beitang sag, where the Mesozoic dominates the bedrock, the depth gradually increasing to the east, with a range of 1500–2500 m (Gao et al., 2000).

Sandstone geothermal reservoirs and carbonate geothermal reservoirs, mainly limestone and dolomite, are developed in the Donglihu area, from top to bottom. The sandstone geothermal reservoir includes the Neoproterozoic Minghuazhen Formation (N*m*) and the Neoproterozoic Guantao Formation (N*g*), the carbonate geothermal reservoir including the Ordovician (O), Cambrian and Wumishan Formation of the Jixian System (J*xw*). The geothermal reservoir of the N*m* is distributed throughout the whole area, with a top depth of 930–1050 m and an average thickness of 506 m, the water output of a single well being 30–100m^3/h and the temperature being 55–80°C. The geothermal reservoir of the N*g* is also distributed throughout the region, with a top depth of 1394–1598 m and a thickness of 36–390 m, the water output from a single well being 90–110 m^3/h and the temperature is 55–59°C. The Ordovician geothermal reservoir is absent from the west side of the Cangdong fault, but is developed on the east side; the top depth of the existing borehole exposed is 1674–3130 m, the thickness is 22–419 m, the water output from a single well is 112–128 m^3/h and the temperature 96–99°C. The Cambrian geothermal reservoir was locally missing from the west side of the Cangdong fault, but developed on the east side. To the east of the Cangdong fault, the top depth of the Cambrian geothermal reservoir is generally greater than 2,000 m, for the Beitang sag area the figure may be greater than 4,000 m, with the thickness of the existing borehole exposure being 10–156 m. The development of this geothermal reservoir is unstable and the water-richness is uneven. The geothermal reservoir of the J*xw* is developed over the whole area. The available borehole data show that the top depth of the west side of the Cangdong fault is 1655–2050 m, with a thickness of 37–1031.81 m (not always determined), while the top depth of the east side is 2042–3482 m, with a thickness of 153–749.58 m (not always determined). Further east to the Beitang sag, the depth of this geothermal reservoir is generally greater than 4,000 m, the water output from a single well being 70–150 m^3/h with a temperature of 92–102°C.

By the end of 2022, three geothermal reservoirs had been utilized in the Donglihu area: the N*m*, the Ordovician System and the J*xw*. When the geothermal wells were drilled, the water output was 53.3 (self-flowing)–204.61 m^3/h and the temperature was 59–102°C. In 2022, the total heating space in the study area was 442.62 × 10^4 m^2, of

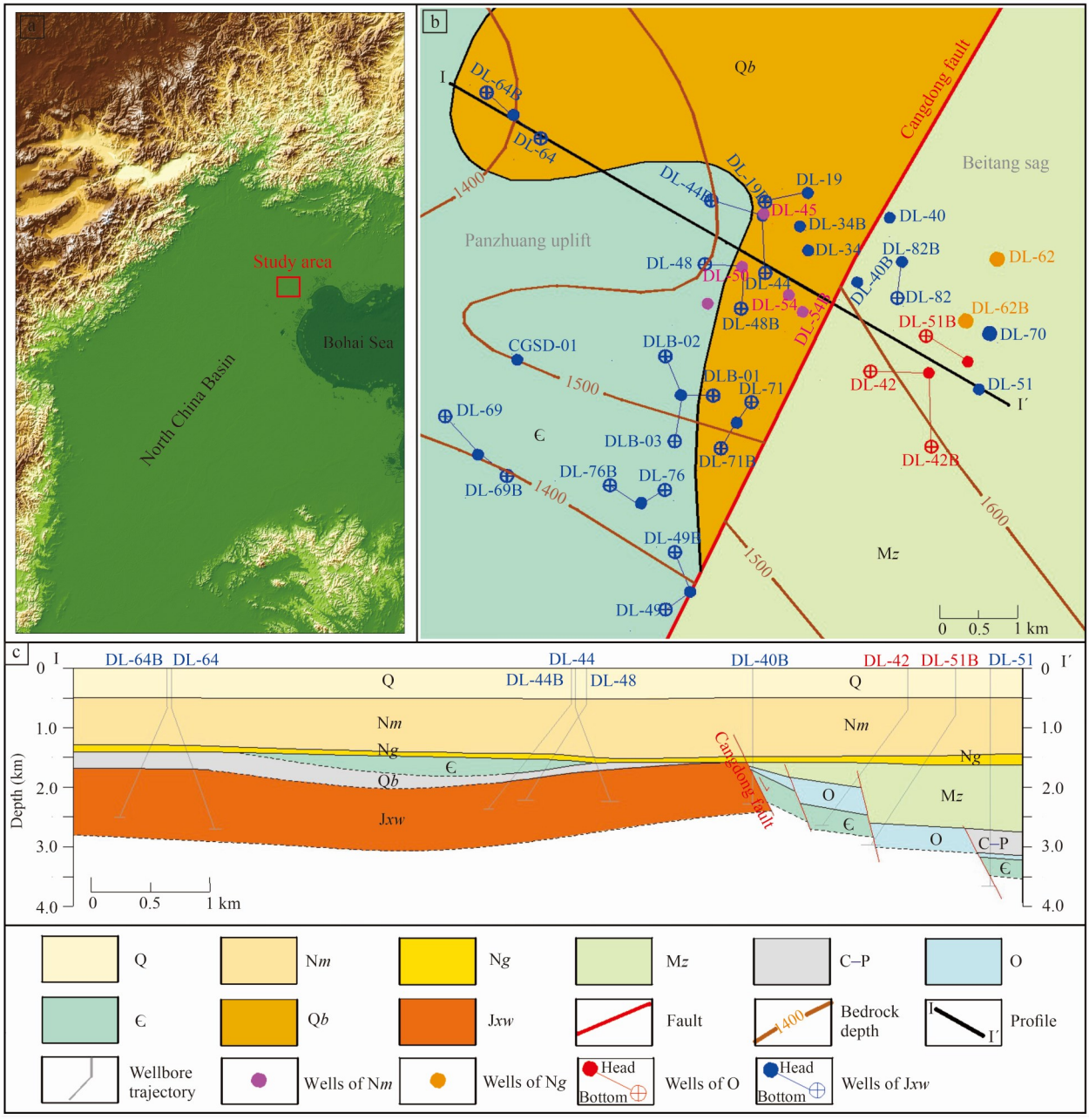

Fig. 1. Bedrock geology map and distribution of geothermal wells in the Donglihu area, northeastern NCB.
Q: Quaternary sedimentary cover; N*m*: sandstone geothermal reservoirs of the Neoproterozoic Minghuazhen Fm.; Ng: sandstone geothermal reservoir of the Neoproterozoic Tantao Fm.; Mz: Mesozoic facies; C–P: Carboniferous and Permian strata; O: Ordovician carbonate geothermal reservoirs; Є: Cambrian carbonate geothermal reservoirs; Q*b*: Neoproterozoic Qingbaikoukou System; J*xw*: carbonate geothermal reservoirs of the Wumishan Fm., Jixian System, middle Archaean.

which 236.24 × 10^4 m^2 came from geothermal heating, accounting for 53.37% of the total heating space.

3 Data and Methods

3.1 Geothermal fluid dynamic monitoring data

Geothermal resources have been used in the Donglihu area since 1999 and, after 24 years of development, a relatively systematic and scientific dynamic routing monitoring system has been established. By October 2022, 39 geothermal wells were included in the monitoring network, including 11 critical monitoring wells. The monitored items include water level depth (the water level beneath the surface), water temperature (wellhead flow and geothermal reservoir temperature), flow rate and water quality. The water level depth is mainly monitored manually, with the measurement error of the portable electronic water table meter and the steel gauge water table meter used being less than 1 cm/100 m, amongst which DL-19 and DL-40 achieve automatic monitoring

Table 1 Annual mean water level depths (m) of typical geothermal wells in different reservoirs

Well ID	Geothermal reservoir	2012	2013	2014	2015	2016	2017	2018	2019	2020	2021	2022
DL-19	J*xw*	105.00	118.00	112.30	117.50	123.90	131.32	134.97	136.25	136.20	129.97	123.95
DL-40	J*xw*	108.50	112.00	116.00	120.87	135.62	132.95	138.33	138.37	137.81	132.29	127.25
DL-42	O	--	110.81	116.50	121.80	128.00	134.94	142.60	140.10	138.90	133.00	128.94
DL-44	J*xw*	--	109.40	114.00	118.36	124.56	131.34	134.00	135.90	134.60	129.56	125.09
DL-50	N*m*	--	--	--	--	--	95.83	--	--	98.00	--	--
DL-51	J*xw*	--	--	--	137.51	134.00	141.52	144.65	142.78	143.26	137.37	132.00
DL-54	N*m*	78.19	82.00	86.00	89.80	95.91	100.86	102.90	101.44	99.51	97.35	93.52
DL-62	Ng	--	87.00	90.47	93.62	97.90	103.01	104.25	106.31	106.15	Stopped	--

Table 2 Pumping and reinjection volumes and reinjection rates of major geothermal reservoirs in the study area during 2013–2022

Year	Pumping volume ($\times 10^4$ m^3)				Reinjection volume ($\times 10^4$ m^3)				Reinjection rate (%)
	N*m*	O	J*xw*	Total	N*m*	O	J*xw*	Total	
2013	8.83	45.24	229.01	283.08	0.00	0.00	107.34	107.34	37.92
2014	2.12	39.48	224.50	266.10	0.00	57.32	144.49	201.81	75.84
2015	19.72	27.94	266.91	314.56	7.68	48.19	202.05	257.92	81.99
2016	12.54	30.14	304.85	347.53	0.00	56.26	202.81	259.07	74.54
2017	52.97	49.79	379.36	482.11	3.78	65.59	203.12	272.49	56.52
2018	56.66	52.20	389.27	498.14	0.00	81.46	232.55	314.01	63.04
2019	59.17	52.63	394.07	505.86	0.05	75.69	264.24	339.98	67.21
2020	50.20	35.05	338.02	423.28	4.91	67.17	255.25	327.34	77.33
2021	56.08	68.58	438.18	562.84	0.00	91.90	383.60	475.49	84.48
2022	38.99	55.20	408.75	502.93	0.00	78.66	363.71	442.37	87.96

with an accuracy of 0.05% FS. Water temperature monitoring includes the water temperature at the time of pumping and the geothermal reservoir temperature under steady-state conditions. Digital thermometers, infrared temperature guns and automated wellhead temperature monitoring devices were applied to measure the wellhead flow temperature. The geothermal reservoir temperature is measured by special logging instruments with a resolution of 0.01°C and a measurement accuracy of 0.5% FS, of which DL-19 and DL-19B, DL-40, DL-69 and DL-69B, DL-82 and DL-82B realize real-time monitoring and automatic data transmission. Flow rate monitoring is automated by an electromagnetic flowmeter (LDG type), with a measurement accuracy of 0.5. Water quality monitoring is carried out for the collection and testing of samples for a complete analysis of monitoring wells, sample collection being carried out in strict accordance with the requirements of 'Collection and Storage of Water Samples for Groundwater Quality Analysis Methods' (DZ/T 0064.2-2021), water quality analysis being completed by the Tianjin Mineral Resources Supervision and Testing Center (Tianjin Geological and Mineral Testing Center) of the Ministry of Land and Resources. Due to the large amount of data involved, only some of the statistical eigenvalues are listed in the text. Time-series water level depths for typical geothermal wells in different geothermal reservoirs are shown in Table 1 and the pump-reinjection data for different geothermal reservoirs are shown in Table 2.

3.2 Steady-state borehole logging data

Logging in a borehole under a steady thermal state is the only way to truly reflect the unified temperature state of the drilling fluid (or the fluid in the well) and the surrounding rock, to definitively reveal the actual original geothermal state of the subsurface rock (Qiu et al., 2019). In recent years, systematic continuous steady-state temperature logging has been carried out in Tianjin (Yin et al., 2024), i.e., continuous temperature logging in geothermal wells during the non-heating period (April–October) to grasp the temperature change of geothermal reservoirs after ceasing pumping-reinjection, which provides the data for studying the characteristics of the regional geothermal field. This study systematically collects the borehole steady-state logging data in the study area. We selected representative geothermal wells, whose utilization has less impact on temperature, for analysis (Table 3). The wellhead flow temperature is the outflow temperature corresponding to the maximum flow rate, after the well is completed. The cap bottom (the bottom of the Guantao Formation, Ng) temperature is the temperature at the bottom of the sedimentary layer during the non-heating period in 2022 (due to the different times and equipment for monitoring the outflow temperature and the cap bottom temperature, there will be some discrepancy between the two temperatures in individual geothermal wells, but it does not affect the analysis of the regional temperature field in this study). The steady-state temperature logging mainly uses the PS-2712 logger, the data being transmitted through the cable and the cable being released at a uniform speed of less than 800m/h while logging.

3.3 Tracer test

3.3.1 Test design

The tracer test involved a total of 15 geothermal wells, including two wells in the N*m* (DL-45 and DL-54) and 13 wells in the J*xw* (DL-19, DL-34, DL-40, DL-44, DL-48, DL-48B, DL-49, DL-64, DL-69, DL-76, DLB-02, DLB-03 and CGSD-01) formations. Well DL-48B was selected as the tracer drop well, the surrounding pumping wells being used as monitoring wells. The geothermal reservoir of the J*xw* was used as the main reservoir for test injection and observation, while the N*m* was used for auxiliary observations. The adsorption test was carried out before

Table 3 Basic information of major geothermal wells in the study area

Well ID	Well depth (m)	Utilization type	Well completion time	Geothermal reservoir	Top of the geothermal reservoir (m)	Wellhead temp. (°C)	Thermal gradient in the cap rocks (°C/100 m)	Temp. of cap bottom (°C)	Temp. of geothermal reservoir (°C)
DL-19B	2384	Reinjection well-stopped	2008-11-24	J*xw*	1818	--	--	--	--
DL-34B	2356	Reinjection well-stopped	2006-6-22	J*xw*	1798	--	--	--	--
DL-40	2328	Pumping well-stopped	2007-1-27	J*xw*	1794	98.5	4.5	93.2	101.0
DL-42	2760	Pumping well-stopped	2008-8-13	O	2053	99.0	3.7	88.1	101.0
DL-44	2252	Pumping well-stopped	2010-7-3	J*xw*	1689	98.0	4.7	91.2	100.2
DL-48	2231	Pumping well-stopped	2011-6-29	J*xw*	1857.89	93.0	4.1	89.0	100.0
DL-49	2546	Pumping well-stopped	2011-10-10	J*xw*	2190	96.0	--	--	--
DL-49B	2398	Reinjection well-stopped	2011-12-21	J*xw*	1848	98.0	--	--	--
DL-50	1510	Pumping well-stopped	2009-10-19	N*m*	532	57.0	--	--	--
DL-51	3634	Pumping well-stopped	2012-1-5	J*xw*	3481	97.0	--	--	--
DL-54	1510	Pumping well-stopped	2012-6-1	N*m*	520	80.0	--	--	--
DL-62	1672	Pumping well - sealed	2013-7-3	Ng	1245	59.0	--	--	--
DL-64	2494	Pumping well-stopped	2013-11-22	J*xw*	1708	90.0	4.2	83.7	97.6
DL-64B	2784	Reinjection well-stopped	2013-10-3	J*xw*	1752	96.0	3.7	77.4	97.6
DL-69	2451	Pumping well-stopped	2014-9-30	J*xw*	1895	94.0	3.4	77.7	--
DL-69B	2666	Reinjection well-stopped	2014-8-13	J*xw*	2042	92.0	3.6	85.7	99.9
DL-71	1905	Pumping well-stopped	2018-10-15	J*xw*	1556	96.0	5.7	101.2	101.2
DL-76	2397	Pumping well-stopped	2015-2-3	J*xw*	1678	91.0	4.9	94.4	101.7
DL-76B	2568	Reinjection well-stopped	2015-2-3	J*xw*	2020	91.0	3.8	88.7	--
DL-82	2438	Pumping well-stopped	2017-1-8	J*xw*	2188	93.0	3.4	87.2	99.2
DLB-01	1904	Reinjection well-stopped	2017-10-7	J*xw*	1676	96.0	5.1	96.8	100.0
DLB-03	2377	Reinjection well-stopped	2018-5-23	J*xw*	1800	94.5	4.5	94.0	100.3

the test, with sodium 1.5-naphthalenesulfonate being selected as a tracer to make a standard solution to react with the rock chips of the J*xw* in the study area at high temperature and high pressure. A high-performance liquid chromatography system was applied to detect the test results, the results showing that the adsorption amount of 1t rock chips to 1.5-naphthalene sulfonic acid sodium was 0.664×10^{-5} g, with a low adsorption rate. Also, the laboratory simulated the hydrolysis of sodium 1.5-naphthalenesulfonate under high temperature and pressure conditions, the results showing that no hydrolysis occurred and that the stability of this tracer was good. Bernard et al. (2004), Rose et al. (2012) and Kristjánsson et al. (2016) have all conducted tracer tests using naphthalenesulfonate as a tracer with good results. Based on the above test results and successful cases with the absence of 1.5-naphthalenesulfonate background values in the target geothermal reservoir (Wang, 2016), it was selected as a tracer in this test. According to the adsorption test results, the tracer concentration in the geothermal reservoir has to be at least 1.0×10^{-9} mol/L to detect the recovery of the tracer, the required tracer quantity being 50 kg, based on the dispersion distance of 2000 m. To ensure the success of the tracer test, the placement amount was 20 times the calculated required tracer, i.e., 1000 kg of sodium 1.5-naphthalenesulfonate.

3.3.2 Sampling and testing

The sampling frequency was divided into three levels, taking into account the geological and structural conditions of the test area, the characteristics of the geothermal reservoir's hydrodynamic field, the target geothermal reservoir, the distance between wells, and the utilization situation. During the pumping period, the sampling frequency of Class I sampling wells was three times per day, Class II sampling wells were sampled once per day and Class III sampling wells were sampled once a week. The sampling wells corresponding to each level are shown in Table 4, where DLB-02, DLB-03 and CGSD-01 were only included in this test during the pressure reduction test, as due to the monitoring conditions they were graded no more, due to the short sampling time.

The tracer test started on January 1, 2018, ending on January 22, 2019. Due to the impact of geothermal utilization, which resulted in discontinuous sampling, water samples were obtained on 110 days, totaling 1274 samples, with several water samples being taken for multiple testing, to ensure the accuracy of the data, the total number of test results being 3000. The test was completed by the Geothermal and Hot Dry Rock Exploration and Development Technology Innovation Center Laboratory of the Ministry of Natural Resources,

Table 4 Classification of sampling wells for tracer test

Sampling frequency levels	Geothermal reservoir	Well ID
I	J*xw*	DL-44, DL-48, DL-69, DL-76
II	J*xw*	DL-19, DL-34, DL-40, DL-49, DL-64
III	N*m*	DL-45, DL-54

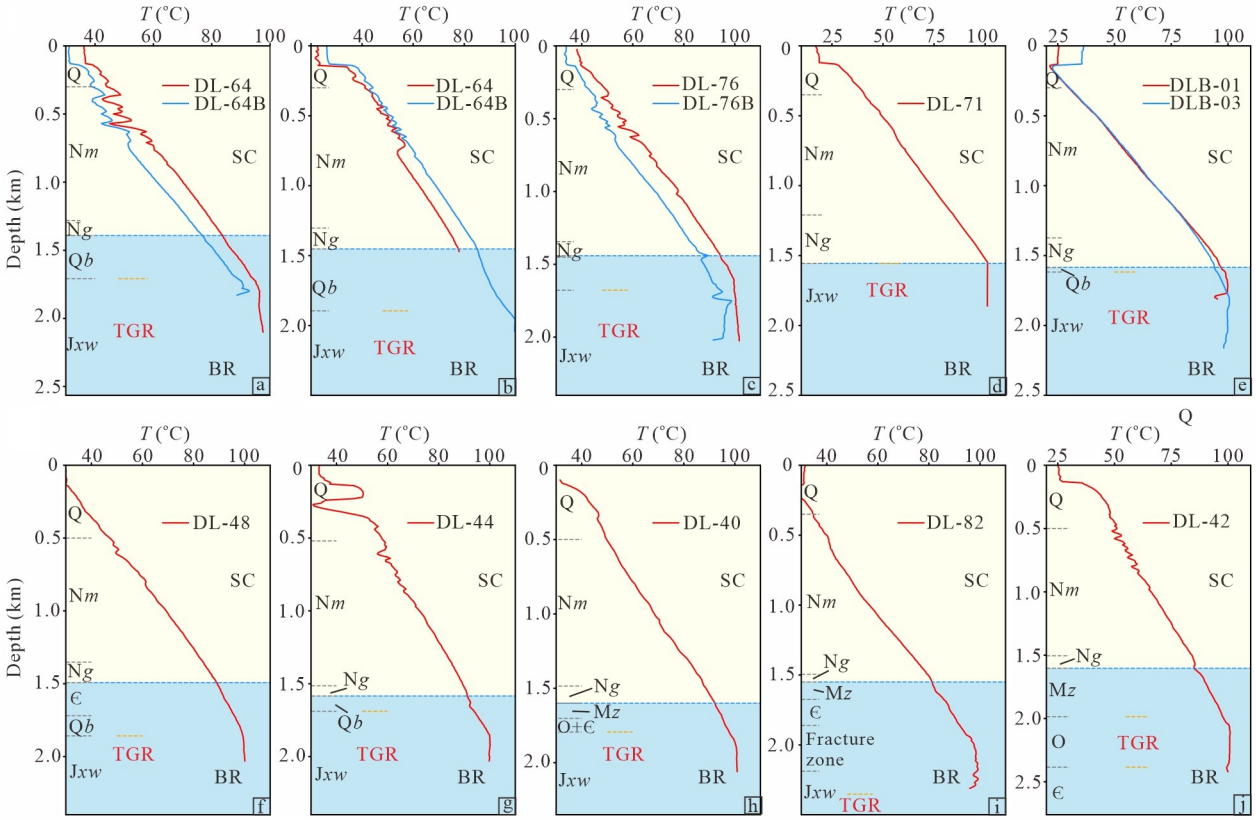

Fig. 2. Steady-state logging curve of geothermal wells or pumping–reinjection system in the study area.
SC: sedimentary cover; BR: bedrock; TGR: target geothermal reservoir.

the instrument used being the Shanghai Tongwei EasySep-1020 liquid chromatography system, with a lower detection limit of 1.0×10^{-9} mol/L.

4 Results

4.1 Steady-state temperature logging results

Some of the geothermal wells in the study area are inclined. The temperature-depth curves of these wells or pumping-reinjection systems were plotted, after correcting the logging data from the borehole inclination, the results being shown in Fig. 2. The curves clearly show the effects of different lithologies, air temperatures and shallow groundwater activity on temperature, with all curves being roughly divided into three parts. The upper part (500m or shallower) is distributed with the Quaternary aquifer. The temperature is more seriously disturbed by shallow air temperature and groundwater, while the linear relationship could be better. The middle part (about 500–1500 m) is mainly Neoproterozoic N*m* and N*g* sandstone geothermal reservoirs, with good temperature-depth linear relationships, reflecting the characteristics of the conductive heat transfer, the temperature increasing linearly with depth. The temperature-depth curve is still linearly increasing at depths greater than 1500m, the rocks being mainly J*xw* and Q*b* siliceous tuffs. However, the geothermal gradient is decreasing, as the thermal conductivity of limestones and dolomites in the basin (2.5–3.35 W/m.k) is significantly higher than that of Cenozoic sandy-muddy sedimentary rocks (1.25–1.67 W/m.k) (Qiu et al., 2019). In addition, the alternating water flow in the barely leaking geothermal reservoir section in the geothermal wells is good, the temperature being homogeneous.

The geothermal gradient refers to the rate of temperature change with depth below Earth's internal thermostatic zone. It is usually expressed as an increase in temperature per 100 m or 1 km. The geothermal gradient of the measured section can be obtained from a linear regression of temperature-depth data within a specific depth section. As can be seen from Fig. 2, all curves are disturbed by shallow groundwater activity or external factors within a specific range from the surface, meaning that the geothermal gradient cannot be calculated, so the temperature-depth linear regression of the temperature measurement data in the undisturbed section is selected to obtain the average geothermal gradient in the cap section (the sedimentary layer above the bottom of Ng) (Table 1; Fig. 2). The geothermal temperature gradients of all cap sections ranged from 3.4–5.7 °C/100 m, with an average of 4.2 °C/100 m.

Comparing the temperature-depth curves of different pumping-reinjection systems (Fig. 2a–c), the changes in the geothermal gradient are essentially the same, the difference being in the temperatures at different depths, especially in the geothermal reservoir. Before entering the geothermal reservoir, the temperature gradient of most

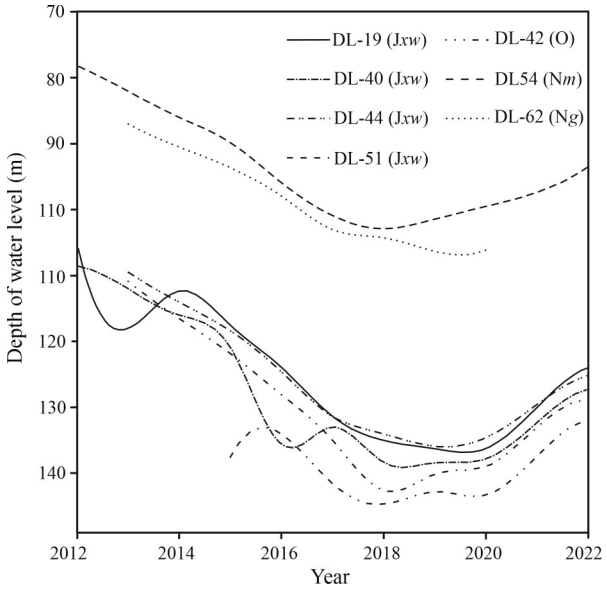

Fig. 3. Water levels of different geothermal reservoirs near the Cangdong fault during 2012–2022, all of which show a yearly decreasing trend in 2018, after which they no longer decrease, beginning to recover in 2020.

reinjection wells is the same as that of the pumping wells. However, the temperature is significantly lower than that of pumping wells at the same level, indicating that the reinjection wells are still affected by the reinjection of colder water during the heating period. The temperature is lower than the original state. After entering the geothermal reservoir, the temperature of the pumping wells shows a slow increase, with a slight gradient. However, there is a decrease in the temperature of the reinjection wells, because of the cold water received from external recharge during the heating period, the temperature recovering slowly, because the volume of cold water stored in the lower karst reservoir with large pores is much larger than the volume of the upper wellbore, while the volume of the water column in the upper wellbore is small. The heated area is large, so it can receive heat from the surrounding rock during the non-heating cycle and gradually recover. Therefore, at the same time, the water temperature in the upper wellbore will gradually approach that of the surroundings. In contrast, the water temperature in the lower karst reservoir is still low, resulting in a temperature drop.

4.2 Water levels in different geothermal reservoirs

Figure 3 shows the curves of different geothermal reservoir water level depths near the Cangdong fault from 2012 to 2022. Due to continuous pumping in the study area for nearly 24 years, the water level depths of the deep bedrock geothermal reservoir have dropped below the overlying sandstone geothermal reservoir. Overall, the dynamic changes of geothermal water level depths can be divided into three stages: 1) A continuously declining stage prior to 2018. Both sandstone geothermal water and bedrock geothermal water pumping increased rapidly during this period, with the total pumping volume increasing from 2.83 million m^3 in 2012 to 4.98 million m^3 in 2018 (Fig. 6). Although the reinjection volume also increased during this period, the overall recharge rate showed a decreasing trend during the three years from 2015–2018, i.e., the consumption volume was continuously increasing, resulting in an overall continuously decreasing trend of water level depths. 2) 2018–2020 is the primary flat phase. With increasing reinjection and shutdown of unlicensed geothermal wells (Yin et al., 2024), the total pumping volume of geothermal water did not increase. The annual pumping volume was maintained at about 5 million m^3 from 2018 to 2019, decreasing to 4.32 million m^3 in 2020, while the reinjection volume increased significantly, the reinjection rate increasing from 63% in 2018 to 77% in 2020. The lack of increase in pumping volume, the increase in reinjection rate and the shutdown of unlicensed geothermal wells significantly reduced the consumption, the recharge generated under the effect of pressure difference with the surrounding water level depths making the water level depths achieve a smooth state, without rising or falling. 3) After 2020 is the overall rebound stage. The total amount of geothermal water pumping does not change much, however the reinjection volume increased significantly, the overall reinjection rate reaching 88% in 2022 and the water level depths of different geothermal reservoirs starting to rise slowly.

Analyzed by different geothermal reservoirs, the pumping volume of the N*m* geothermal reservoir remained unchanged during 2017–2020, maintaining an average of about 550,000 m^3 per year, dropping to 390,000 m^3 by 2022, while its reinjection rate has remained at a low level, in recent years being 0 (Fig. 4a). The reinjection rate of the Ordovician geothermal reservoir has been maintained at a high level, due to the ease of reinjection and acceptance of tailwater reinjection from other reservoirs (Fig. 4a), with an average reinjection rate of 156% during 2014–2022. The reinjection rate of the Jx*w* reservoir has experienced a 'medium-low-high' trend over the years (Fig. 4a), first decreasing from 75% in 2015 to 53% in 2017, then increasing to 89% in 2022, which corresponds to the change in its water level depths.

4.3 Major anions and cations in different geothermal reservoirs

The Piper diagram of the water quality of different reservoirs is shown in Fig. 5. The cations of the N*m* reservoir are dominated by Na^+, followed by Ca^{2+} and K^+, the anions being dominated by HCO_3^-, followed by Cl^-; Na^+ dominates the cations of the N*g* reservoir, HCO_3^- dominating the anions; the cations of Ordovician and Jx*w* bedrock reservoirs are dominated by Na^+, followed by K^+ and Ca^{2+}, the anions being dominated by HCO_3^- and Cl^- (Fig. 6).

4.4 Trace test results

Of the 14 sampled wells used for testing, six wells (DL-34, DL-44, DL-45, DL-49, DL-69 and CGSD-01) had tracer recovered at concentrations lower than the lower limit of detection (LLOD), with the results being counted

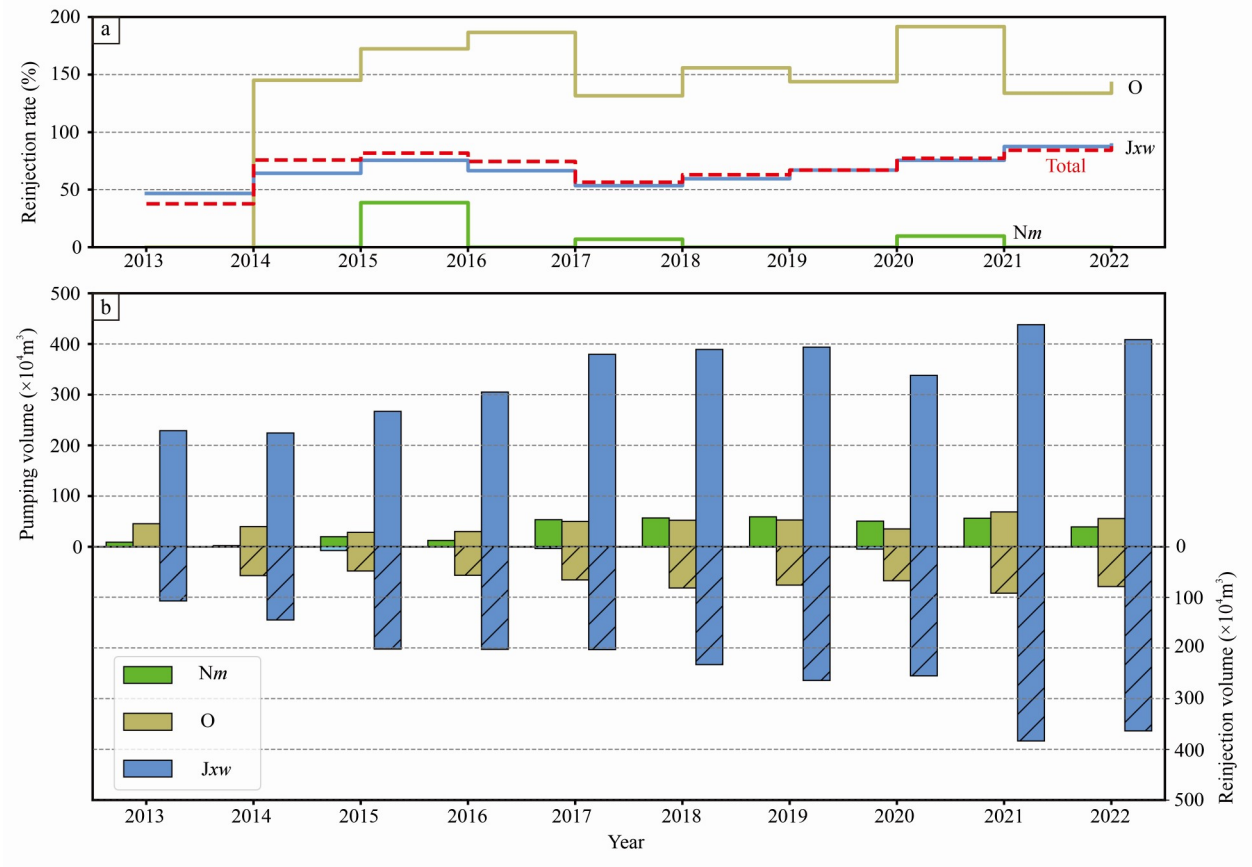

Fig. 4. Pumping and reinjection volume and reinjection rate of major geothermal reservoirs during 2013–2022.

Table 5 Summary of results of tracer test interpretation

Summary	DL-19	DL-40	DL-48	DL-64	DL-76	DLB-02
Date of first arrival of tracer	2018-1-7	2018-1-4	2018-1-4	2018-2-2	2018-2-1	---
Time to first arrival of tracer (d)	6	3	3	32	31	---
Recovery quantity (kg)	0.0052	0.00248	0.0323	0.00127	0.007	⩾0.0309
Recovery rate (× 10^5%)	52.0	24.8	323.0	12.7	67.4	⩾309

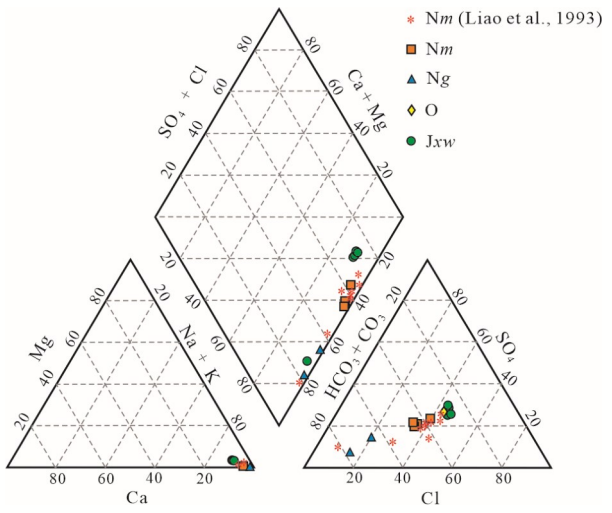

Fig. 5. Piper diagram of geothermal fluids in different geothermal reservoirs near the Cangdong fault.

as zero, the remaining seven wells (DL-19, DL-40, DL-48, DL-54, DL-64, DL-76 and DLB-02) all having recovered tracer (Table 5). Amongst them, DL-54 is a thermal reservoir of the Minghuazhen Formation and tracer was detected in one group of its samples. Although the concentration of tracer is very low, only 6.4 × 10^{-8} kg/m^3, it also indicates that the Cangdong fault (or its secondary fracture) in the study area connects the upper Minghuazhen Formation geothermal reservoir and the lower Wumushan Formation geothermal reservoir.

5 Discussion

5.1 The effect of fracture on the temperature of the geothermal field

5.1.1 Characterization of the temperature field in the top cap rocks

The geothermal field is the temperature distribution of each point in space within the earth at a specific instant, where the distribution of the geothermal field can reflect not only the horizontal distribution of the geothermal

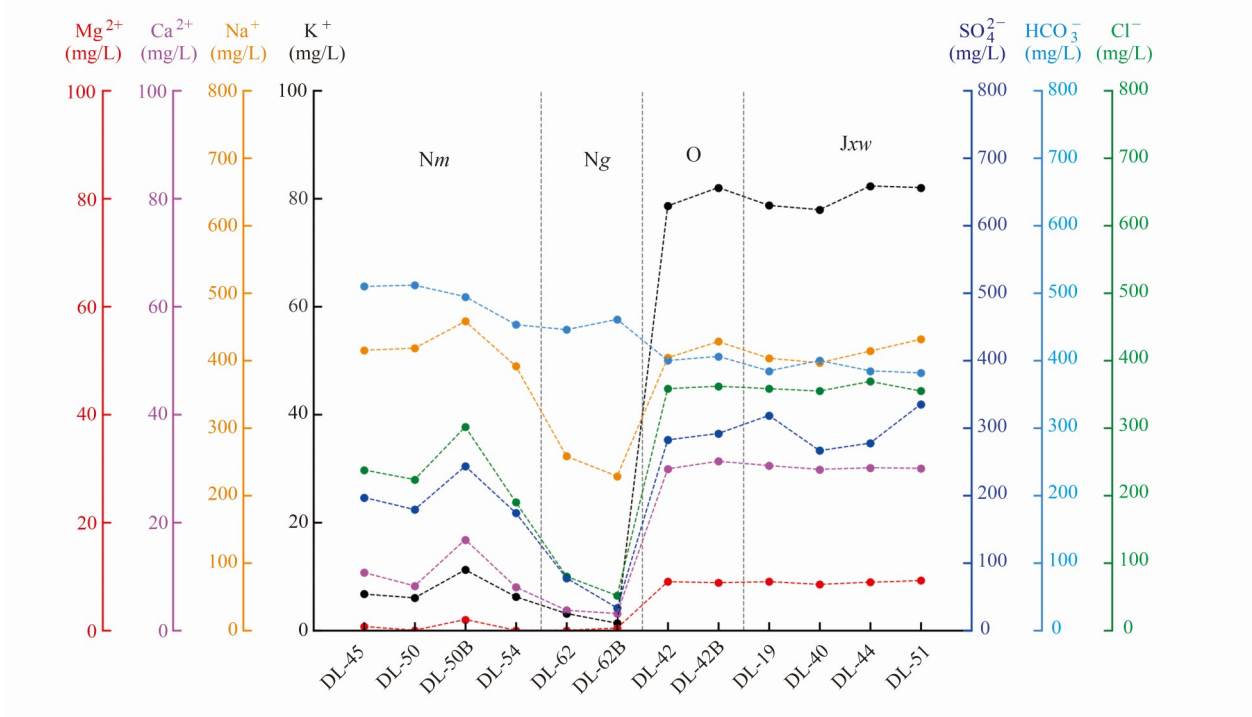

Fig. 6. Major ion contents of different geothermal reservoirs.

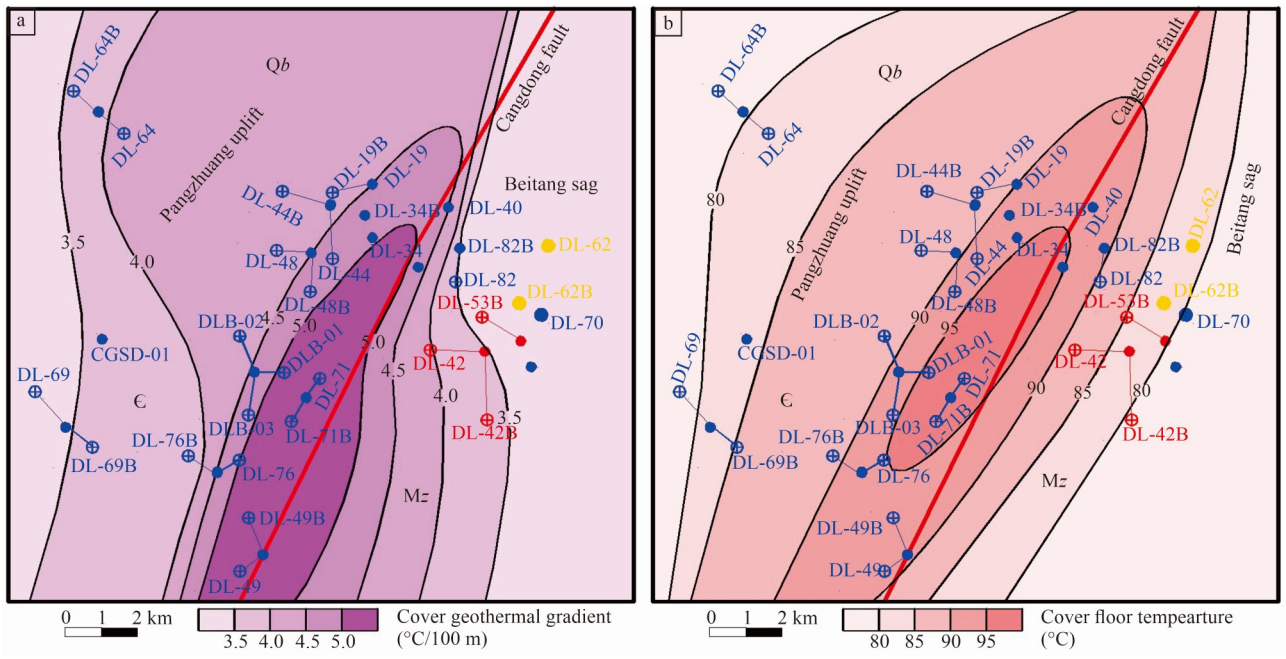

Fig. 7. Distribution of the geothermal field in the study area.
(a) Contours of geothermal gradients in the cap rocks; (b) contours of the temperature at the bottom of the cap rocks.

reservoir, but also the connection characteristics of the geothermal reservoir channels in a vertical direction. The cap temperature gradient contours (Fig. 7a) and the bottom temperature contours (Fig. 7b) of the cap were prepared, based on the steady-state logging data. The results show that the cap temperature gradient ranges from 3.4–5.7 °C/100 m, with the high-value area being located near the Cangdong fault, spreading nearly north-south and gradually decreasing from >5.0 °C/100 m in the high-value area (wells DLB-01 and DL-71) to less than 3.5 °C/100 m (wells DL-69 and DL-82) from east to west (Fig. 7a). The temperature at the bottom of the cap rocks in the study area varies between 77.4 and 101.2°C. The high-value area is located near the Cangdong fault, parallel to the

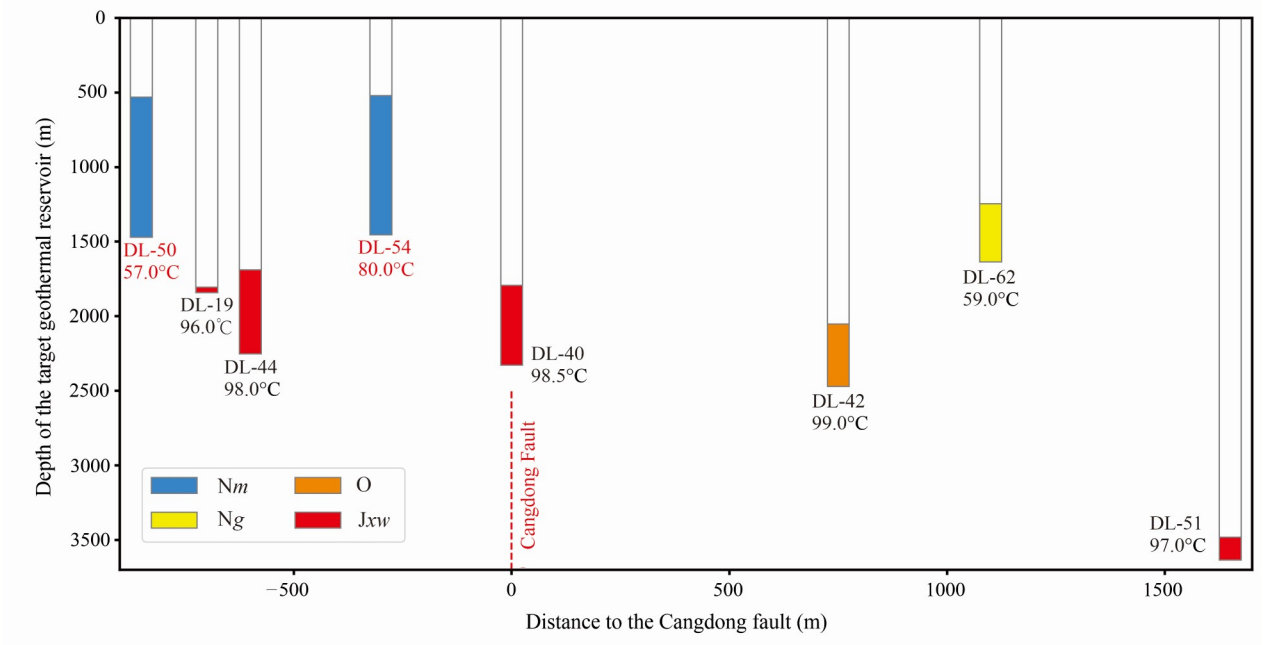

Fig. 8. Water temperature at the wellhead of geothermal wells at different distances from the Cangdong fault, showing that the geothermal wells located near the fault within the same geothermal reservoir have higher water temperatures.

fracture and spreading northeast. It gradually decreases from >95°C in the high-value area (wells DLB-01 and DL-71) to <80°C in the near-vertical fault direction on the east and west sides (wells DL-64B and DL-69) (Fig. 7b). On the whole, the pattern of temperature gradient contours of the cap rocks and the bottom of the cap rocks is generally consistent, with the Cangdong fault as the center and gradually decreasing to the east and west, which shows that the Cangdong fault has a specific thermal control effect on the nearby geothermal reservoir.

5.1.2 Characterization of the temperature field in different geothermal reservoirs

Comparing the wellhead flow temperature (water discharge temperature at completion) of geothermal wells at different distances on both sides of the Cangdong fault (Fig. 8), the temperature distribution has the same pattern. The highest temperature of the J*xw* geothermal reservoir is in well DL-40 near the Cangdong fault, which is 2328 m deep and has a target geothermal reservoir section 1794–2328 m deep, with a wellhead flow temperature as high as 98.5°C. In contrast, well DL-51, about 1650m southeast of the Cangdong fault, is 3634m deep and has a deeper target geothermal reservoir section (3481–3634 m), but its wellhead flow temperature is only 97°C. This may be because deep wells have an extended wellbore, and the hot water exchanges with the surrounding rocks and shallow groundwater more during the ascent, thus lowering the wellhead flow temperature. On the other hand, it may also be due to vertical convection in the fracture zone of the Cangdong fault, which brings the deeper and higher temperature fluids to the shallow part and makes the geothermal wells near the fracture have a higher wellhead flow temperature. The N*m* geothermal well DL-54, located on the west side of the Cangdong fault, further reflects the role of the Cangdong fault as a vertical hydrothermal channel. This well is located about 300 m from the northwest vertical extent of the Candong fault, with a depth of 1510 m. The target geothermal reservoir section is 520–1454 m deep, while the wellhead flow temperature is as high as 80°C, much higher than the wellhead flow temperature range of 48–56°C in most of Tianjin for N*m* geothermal wells, as well as higher than that of the distant N*m* geothermal well DL-50 (about 850 m from the northwest of the Candong fault, with a wellhead flow temperature of 57°C) and N*g* geothermal well DL-62 (about 1100 m to the southeast of the Cangdong fault, with a wellhead flow temperature of 59°C).

From the temperature monitoring data of J*xw* geothermal wells, with the exception of DL-64B, which is affected by reinjection and has a low temperature, the temperature of the other J*xw* geothermal wells ranged from 97.6 to 101.7°C. Geothermal wells with temperatures greater than 101°C and shallow depths are located on the Cangdong fault, including wells DL-40, DL-71 and DL-76. This further verifies the existence of vertical convection in the Cangdong fault zone, which brings higher temperature fluids from the deeper part to the shallower part, making the geothermal wells near the fracture have higher temperatures than other wells.

5.2 The effect of fracture on the water levels of the geothermal reservoir

In addition to the essential characteristics of the hydrodynamic field of normal temperature groundwater, the hydrodynamic field of the hot water system is unique, because the density of hot water decreases with the

increase in temperature. Generally, the deeper the reservoir, the higher the head pressure in the reservoir, the hydraulic head in the pore far from the water control fracture zone gradually decreasing. Comparing the pumping-reinjection of N*m*, Ordovician and J*xw* reservoirs (Fig. 4b) with the overall trend of water level change (Fig. 3) indicates a particular hydraulic connection between different reservoirs. Disregarding the linkage between reservoirs caused by the unregulated construction of geothermal wells in different reservoirs (where it exists, this amount is small), this large-scale synergistic change in water levels in different reservoirs can only be caused by regional deep major fractures that bridge the upper and lower reservoirs.

5.3 The effect of fracture on the water chemistry of geothermal reservoirs

The chemical composition of geothermal water is the result of a long geological process of groundwater evolution and the chemical characteristics of geothermal water can be studied to analyze the formation and evolutionary process of the hot water (Yu et al., 2022; Wang L et al., 2023; Lu et al., 2024; Li et al., 2024). Combined with the Piper diagram (Fig. 5), the N*m*, Ordovician and J*xw* reservoirs are all mainly HCO_3·Cl-Na type water, while the N*g* reservoir is HCO_3-Na type water. The TDS of geothermal well DL-54 in the Minghuazhen Formation is 1286.2 mg/L, while that of geothermal well DL-62 in the Guantao Formation, which is farther away from the Cangdong fault, is 919.7 mg/L. Geothermal wells at shallower depths of thermal reservoirs have higher TDS, which is inconsistent with the tendency of hot water in the majority of the North China Plain to have an increase in TDS from shallower depths to deeper depths. Liao et al. (1993) systematically conducted water quality tests of different reservoirs prior to the large-scale exploitation of geothermal water in the north of the Cangxian uplift. The water quality of the N*m* reservoir that they obtained was plotted on Piper diagrams (Fig. 5), it can be showing that the water quality of the N*m* has remained stable for thirty years, without significant changes. The high TDS of the N*m* reservoir is related to the geological environment during its formation and its long geological evolution, so cannot be used to indicate that it has mixed with the deep bedrock geothermal reservoir through the fracture.

The results of the tracer tests also confirm that the Cangdong fault has a linking effect on the geothermal reservoirs at different depths. The well DL-54 is a N*m* reservoir and one set of samples detected tracer on March 14, 2018, with a concentration of 6.4 $\times 10^{-8}$ kg/m^3, which is low but also indicates that the Cangdong fault (or its secondary fracture) is more developed within the study. The fracture connects the upper N*m* and lower J*xw* reservoirs and has some water conductivity. A tracer test was also conducted in December 2015, with well DL-48B also being selected as the tracer drop well, but 700 kg of ammonium molybdate was injected. No significant tracer was found in the water samples during the 90-day tracer test (Wang, 2016), which is consistent with the extremely low tracer recovery from the results of the current test.

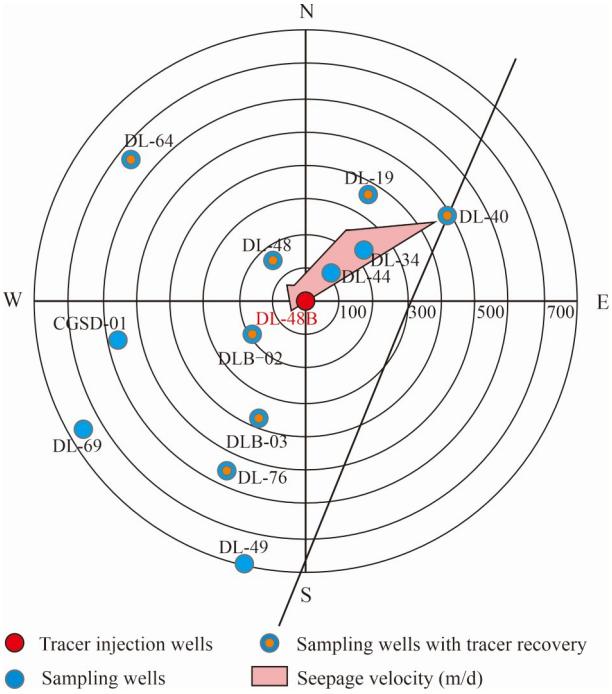

Fig. 9. The radar map shows the dominant direction of seepage in the geothermal reservoir, i.e., NNE, which is consistent with the direction of development of the Cangdong fault and its secondary fracture.

Vertically developed fracture zones and fractures in horizontal rock formations may form the dominant channels for seepage. A radar map of seepage velocity was drawn, based on the tracer test results, as shown in Fig. 9. From the analytical results of the water samples, the maximum flow velocity in the reservoir seepage channels under the development and utilization conditions at that time was 448.42 m/d, the direction of the dominant channel being mainly concentrated in a northeasterly direction. According to tectonic and geological conditions, the Cangdong fault and its secondary fractures are more developed. The fractures are mainly developed along a north-northeast direction, which is consistent with the dominant channel's extension direction, as obtained from the tracer test. In other words, the tectonic and geological conditions and the tracer test results are mutually verified. Meanwhile, the overall water flow direction of the J*xw* reservoir before and after the tracer test (before and after the heating period) is north-east (Fig. 10), which is consistent with the direction of the dominant channel obtained from the tracer test, so it further authenticates that the main groundwater runoff direction of the J*xw* reservoir is to the north-east.

The Cangxian uplift is located in the northeastern part of the NCB, which is influenced by the subduction of the western Pacific plate and the demolition of the North China Craton lithosphere, the strong subsidence since the Paleozoic making the region have the thinnest lithosphere (60–80 km) and crustal thickness (<35 km) in the North China Craton. The lithospheric thinning and the upwelling

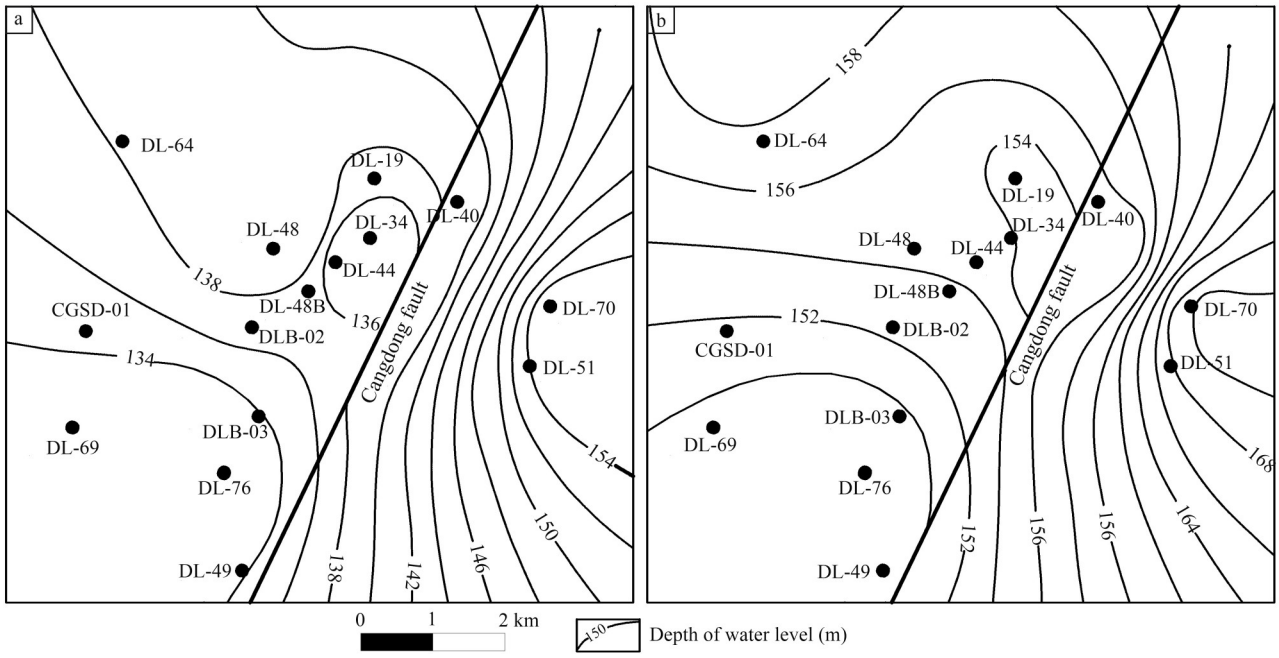

Fig. 10. Depth of geothermal water tables in the study area before and after the winter heating season (geothermal water centralized pumping period, from November 15 to March 15 of the following year), the contours showing that the geothermal water in the J*xw* geothermal reservoir in the region flows mainly from southwest to northeast.

of mantle thermal material form a local geothermal anomaly, which provides a high temperature thermal background for the formation of geothermal resources in the region. The uplift and depression pattern formed by the undulation of the basement bedrock surface of the basin plays a regulatory role in the regional geothermal field and the distribution of surface heat flow (Chen, 1988; Xiong and Zhang, 1988). The Cangdong fault is produced on the backslope composed of Paleozoic strata, which is a product of the Indosinian–Yanshanian rotation. The fracture activity controls the Mesozoic and Cenozoic sedimentation and is an important hidden fracture in Tianjin, constituting the main boundary fracture shared by the Huanghua depression and the Cangxian uplift in the Bohai Bay basin, its formation and evolution being closely related to the development of the Bohai Bay basin, especially the Huanghua depression (Wu and Li, 1994; Gao et al., 2000). According to the velocity structure profile of the upper mantle of the crust that crosses the northern part of the Cangdong fault, as obtained by the Geophysical Exploration Center of the National Seismological Bureau using the deep seismic wide-angle reflection/refraction detection technique, the Cangdong fault is a large detachment fracture developed in the upper crust, which is an intracrustal fracture and does not penetrate the crust (Fig. 11). It, therefore, does not have the structural condition of a heat convection channel for large-scale upward 'transportation' of deep mantle heat. Comparing the steady-state logging results in the Donglihu area, the temperature gradient in the cover section of the different geothermal wells is in the range 3.4 –5.7 °C/100 m. Although the high-value area is shown in the plane between the Cangdong fault and the Inner Cangdong fault and spreads northeast, the influence is limited. It would be expected that the heat in the relatively deep reservoir is transferred to the shallower part of the fracture zone in the form of convection, thus exerting some influence on the temperature field within the fractured zone. However, its effect diminishes and disappears as it moves away from the fracture zone. According to the geochemical exploration results of the hidden fracture in Gegu, Tianjin, the top of the Candong fault breaks into the middle Pleistocene but not the upper Pleistocene in Tianjin, i.e., the Candong fault communicates with the main reservoirs in the study area, such as the N*m*, N*g*, Ordovician and J*xw*, thus acting as a water flow channel between the upper and lower reservoirs in the local area and playing a specific 'heat transport' role (Fig. 12).

6 Conclusions

Comparative analysis of the long-term dynamic monitoring data of different geothermal reservoirs in the Cangxian uplift within the North China Basin reveals that the water levels of different geothermal reservoirs show a consistent trend. Given the different pumping strengths of different reservoirs, it is inferred that such a wide range of coordinated water level changes may be caused by the hidden fractures in the deep part of the basin communicating between the upper and lower reservoirs. Further geothermal water chemical analysis and tracer tests confirm that the deeply hidden fracture in the area connects the upper part of the Minghuazhen sandstone

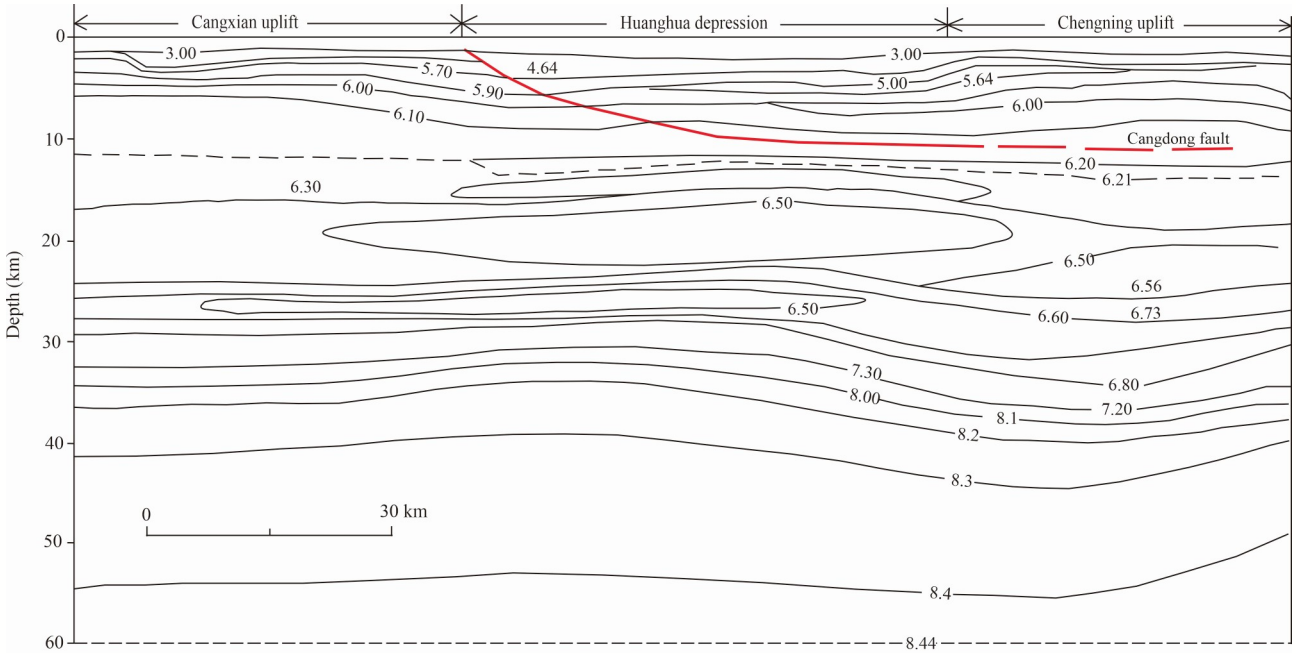

Fig. 11. P-wave velocity (km/s) in the crust and upper mantle of the Cangxian uplift and Huanghua depression (modified after Zhao et al., 2007).
The red line in the figure shows the velocity excursion zone, which is presumed to be the Cangdong fault.

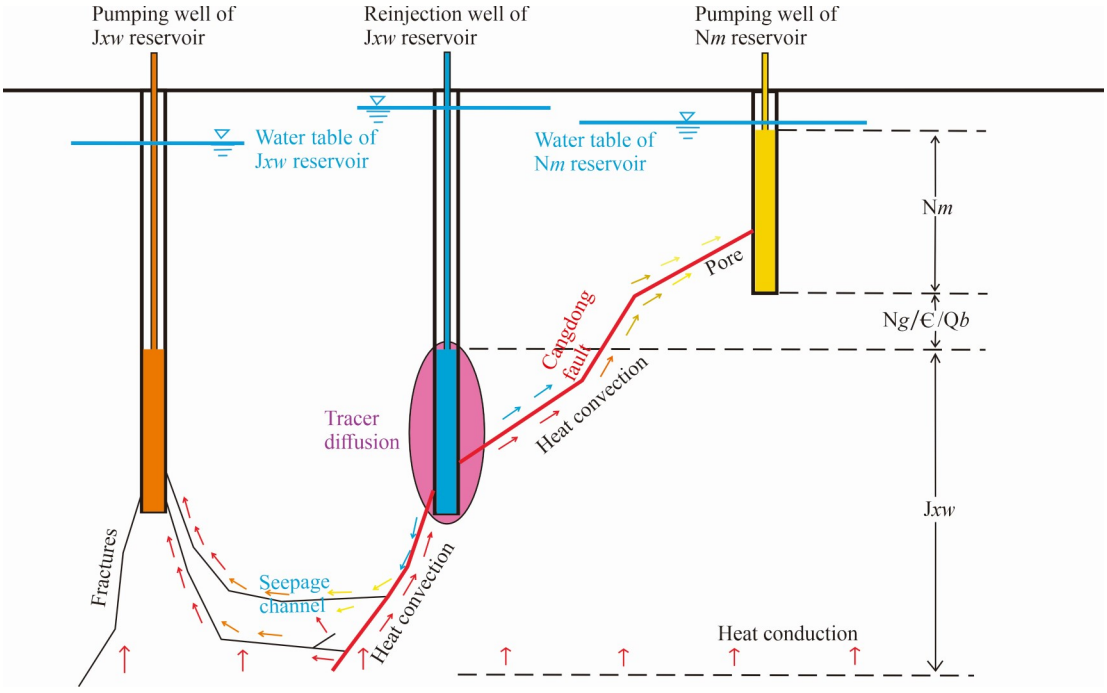

Fig. 12. Schematic diagram of the Cangdong fault as a hydrothermal channel for geothermal reservoirs at different depths.

geothermal reservoir and the lower part of the Wumishan carbonate geothermal reservoir, with a certain degree of hydraulic conductivity. The seepage channel is mainly north-east, in the direction of the Cangdong fault. The temperature is also affected by the convection of hot water in the fracture zone. The spatial distribution of the temperature gradient in the sedimentary cover is spreading in a northeasterly direction. Its high-value area is distributed around the Cangdong fault. The geothermal reservoir temperatures at different depths are reduced from

the Cangdong fault to both sides. However, the influence range is limited, its effect is gradually weakened and disappears once it is far away from the fracture zone. Taking into account the comprehensive temperature characteristics, the water level of different geothermal reservoirs, water chemistry and tracer test data, the following can be concluded: the Cangdong fault communicates with different geothermal reservoirs in the shallow part and plays a specific role in the 'water-heat' channel in the local area.

This study attempts to explore the hydrothermal regulatory role of the deep hidden fracture in the sedimentary basin from various aspects, such as geothermal water chemistry, hydraulic head and geothermal reservoir temperature, etc. The related understanding has a certain theoretical significance for further deepening understanding of the mechanism of geothermal genesis in the sedimentary basin, but it also has a specific practical significance for the development of geothermal resources in the sedimentary basin. When constructing geothermal wells in similar areas in the future, the role of this fracture in connecting water and heat to the upper and lower reservoirs should be considered.

Acknowledgments

This work was funded by Public Interest Monitoring Project (No. XCSD-2024-317) of the Tianjin Municipal Bureau of Planning and Natural Resources.

Manuscript received Jun. 24, 2023
accepted Apr. 19, 2024
associate EIC: XU Tianfu
edited by Jeffery J. LISTON and FEI Hongcai

References

Bernard, S., Peter, R., Jean-Claude, F., Michel, B., and Gilles, B., 2004. Tracer testing at Soultz-Sous-Forets (France) using Na-Benzoate,1,5 and 2,7 Naphthalene Disulfonate. Proceedings, 29th Workshop on Geothermal Reservoir Engineering Stanford University, Stanford, California, January 26–28, SGP -TR-175.

Chen, M., 1988. Geothermics of North China. Beijing: Science Press (in Chinese).

Chen, M., and Wang, J., 1994. Geothermal resources in China: formation characteristics and potential assessment. Beijing: Sciences Press, 1–252 (in Chinese with English abstract).

Gao, Z.W., Xu, J., and Song, C.Q., 2000. Structural characters of the Cangdong fault in North China. Seismology and Geology, 22(4): 395–404 (in Chinese with English abstract).

Hao, Y.W., Luo, M.S., Xu, Z.L., Zou, Y.R., and Tang, T.T., 2014. Division of sedimentary basins and its tectonic evolution in North China from Newproterozoic to Mesozoic. Earth Science, 39(8): 1230–1242 (in Chinese with English abstract).

Kristjansson, B.R., Axelsson, G., Gunnarsson, G., Gunnarsson, I., and Oskarsson, F., 2016. Comprehensive tracer testing in the Hellisheidi geothermal field in SW-Iceland. Proceedings, 41st Workshop on Geothermal Reservoir Engineering Stanford University, Stanford, California, February 22–24, SGP-TR-209.

Li, T., Lu, R., Xie, W., Zhu, J., Liu, L., and Lin, W., 2024. Fluid chemical and isotopic signatures insighting the hydrothermal control of the Wahongshan–Wenquan Fracture Zone (WWFZ), NE Tibetan Plateau. Energies, 17(11): 2715.

Liao, Z.J., and Chen, Z.X., 1993. Thermal water of Shanlingzhi geothermal field, Tianjin. Acta Scicentiarum Naturalum Universitis Pekinesis, 29(2): 224–232 (in Chinese with English abstract).

Lin, W., Wang, G., Gan, H., Zhang, S., Zhao, Z., Yue, G., and Long, X., 2022. Heat source model for Enhanced Geothermal Systems (EGS) under different geological conditions in China. Gondwana Research, 122: 243–259.

Lin, W.J., Wang, G.L., Shao, J.L., Gan, H.N., and Tan, X.F., 2021a. Distribution and exploration of hot dry rock resources in China: Progress and inspiration. Acta Geologica Sinica, 95 (5): 1366–1381 (in Chinese with English abstract).

Lin, W.J., Wang, G.L., Zhang, S., Zhao, Z., Xing, L., Gan, H., and Tan, X., 2021b. Heat aggregation mechanisms of hot dry rocks resources in the Gonghe Basin, northeastern Tibetan Plateau. Acta Geologica Sinica (English Edition), 95(6): 1793–1804.

Long, X., Wang, G., Lin, W., Wang, J., He, Z., Ma, J., and Yin, X., 2023. Locating geothermal resources using seismic exploration in Xian County, China. Geothermics, 112: 102747.

Lu, R., Xie, W., Liu, B., Zhang, S., Zhu, J., and Lin, W., 2024. Geothermal fluid chemistry and isotope for interpreting the formation of complex geothermal system in the Gonghe Basin, northeastern Tibetan Plateau, Journal of Hydrology, 633: 130813.

Mao, X.P., 2018. Genetic mechanism and distribution characteristics of high temperature anomaly in geothermal field. Acta Geoscientica Sinica, 39(2): 216–224 (in Chinese with English abstract).

Mohammad, A. A., 2021. Tectonic and Structural Controls on Geothermal Systems. In: Shandilya, A.K. et al. (eds.), Geological and Geo-Environmental Processes on Earth, Springer Natural Hazards.

Qiu, N., Hu, S., and He, L., 2019. Geothermics in Sedimentary Basins. Beijing: China University of Petroleum Press (in Chinese).

Rose, P., Leecaster, K., Clausen, S., Sanjuan, R., Ames, M., Reimus, P., Williams, M., Vermeul, V., and Benoit, D., 2012, A Tracer test at the Soda Lake, Nevada geothermal field using a sorbing tracer. Proceedings, 37th workshop on Geothermal Reservoir Engineering Stanford University, Stanford, California, January 30- February 1, SGP-TR-194.

Shi, H., Wang, G., Zhang, W., Ma, F., Lin, W., and Ji, M., 2023. Predicting the potential of China's geothermal energy in industrial development and carbon emission reduction. Sustainability, 15(9): 7508.

Wang, G.L., and Lin, W.J., 2020. Main hydro-geothermal systems and their genetic models in China. Acta Geologica Sinica, 94(7): 1923–1937(in Chinese with English abstract).

Wang, G.L., Lin, W.J., Liu, F., Gan, H., Wang, S., Yue, G., Long, X., and Liu, Y., 2023. Theory and survey practice of deep heat accumulation in geothermal system and exploration practice. Acta Geologica Sinica, 97(3): 639–660 (in Chinese with English abstract).

Wang, L., Xing, L., Lin, W., Zhang, W., Zhao, Z., Zhao, J., and Zhai, T., 2023. Chemical characterization and genesis of thermal reservoir water in the southern part of the Jizhong depression. Water, 15(20): 3532.

Wang, L., Liu, K., Ma, Y., Zhang, Y., Tong, J., Jia, W., Zhang, S., and Sun, J., 2024. Geochemical and isotopic techniques constraints on the origin, evolution, and residence time of low-enthalpy geothermal water in western Wugongshan, SE China. Acta Geologica Sinica (English Edition), 98(3): 801–818.

Wang, T.H., Wang, X.W., Mao, X., Luo, L., Gao, N.A., Liu, H.Y., and Wu, C., 2022. Characteristics and development potential of geothermal resources in northern Cangxian uplift. Geology in China, 49(6): 1747–1764 (in Chinese with English abstract)

Wang, W., 2016. Modelling of tracer tests in a geothermal reservoir in Tianjin, China, Report 41 in: Geothermal training in Iceland 2016, UNU-GTP, Iceland, 891–910.

Wang, X.W., Gao, N.A., Wang, T.H., Liu, H.Y., Mao, X.P., and Huang, X., 2022. Distribution characteristics and genetic mechanism of the geothermal abnormality in the Xianxian geothermal field, Hebei Province. Acta Geologica Sinica, 96 (7): 2611–2625 (in Chinese with English abstract).

Wu, T., and Li, Z., 1994. An analysis of property of Cangdong fault. Acta Petrolei Sinica, 15(3): 19–25 (in Chinese with English abstract).
Xiong, L.P., and Zhang, J.M., 1988. Relationship between geothermal gradient and the relief of basement rock in North China plain. Chinese Journal of Geophysics, 31(2): 146–155 (in Chinese with English abstract).
Yin, X.X., Zhao, S.M., Cai, Y., Yan, J.X., and Xu, L., 2024. Dynamics of geothermal reservoirs for intensive geothermal development in Tianjin from 1992 to 2021. Acta Geologica Sinica, 98(1): 297–313 (in Chinese with English abstract).
Yu, M., Wang, G., Ma, F., Zhang, W., Lin, W., Zhu, X., and Zhang, H., 2022. Geochemical characteristics of geothermal fluids of a deep ancient buried hill in the Xiong'an New Area of China. Water, 14(19): 3182.
Zhang, Q., Zhu, X., Wang, G., and Ma, F., 2023. Characteristics, formation periods, and controlling factors of tectonic fractures in carbonate geothermal reservoirs: A case study of the Jixianian System in the Xiongan New Area, China. Acta Geologica Sinica (English Edition), 97(6): 1625–1639.
Zhang, W., Wang, G., Liu, F., Xing, L., and Li, M., 2019. Characteristics of geothermal resources in sedimentary basins. Geology in China, 46(2): 255–268 (in Chinese with English abstract).
Zhao, S., Sun, B., Lin, L., Lin, J., and Ma, Z., 2013. Exploration, development and utilization of sedimentary basin-type geothermal fields. Beijing: Geology Press, 1–293 (in Chinese).
Zhao, S.M., Gao, B.Z., Li, X.M., Li, H.J., and Hu, Y., 2007. Characteristics and water-temperature conductivity of the Cangdong fault (Tianjin Segment). Geological Survey and Research, 30(2): 121–127 (in Chinese with English abstract).

About the first author

YIN Xiaoxiao, female, born in 1990 in Zaozhuang, Shandong Province; master; graduated from the Institute of Disaster Prevention. She is currently an engineer at the Tianjin Geothermal Exploration and Development Design Institute, mainly engaged in geothermal dynamic monitoring research. E-mail: yinxiaoxiaogw@163.com.

About the corresponding author

LIN Jianwang, male, born in 1970; professor-level senior engineer; mainly engaged in geothermal resource exploration and development-related research. E-mail: tjlinjianwang@163.com.